

Lighter and Stronger: Cofabricated Electrodes and Variable Stiffness Elements in Dielectric Actuators

Egor Piskarev, Jun Shintake, Vivek Ramachandran, Neil Baugh, Michael D. Dickey,* and Dario Floreano*

The inherent compliance of soft robots often makes it difficult for them to exert forces on surrounding surfaces or withstand mechanical loading. Controlled stiffness is a solution to empower soft robots with the ability to apply large forces on their environments and sustain external loads without deformations. Herein, a compact, soft actuator composed of a shared electrode used for both electrostatic actuation and variable stiffness is described. The device operates as a dielectric elastomer actuator, while variable stiffness is provided by a shared electrode made of gallium. The fabricated actuator, namely variable stiffness dielectric elastomer actuator (VSDEA), has a compact and lightweight structure with a thickness of 930 μm and a mass of 0.7 g. It exhibits a stiffness change of $183\times$, a bending angle of 31° , and a blocked force of 0.65 mN. Thanks to the lightweight feature, the stiffness change per mass of the actuator ($261\times\text{g}^{-1}$) is 2.6 times higher than that of the other type of VSDEA that has no shared electrode.

unpredictable environments because they are often built with rigid materials with pre-determined functions and limited degree-of-freedom movement. In addition, when such robots interact with soft materials, such as humans, they can even be dangerous.^[2] Over the past decade, there has been a growing interest in developing soft robots that mimic nature, including human muscles. These soft robots are motivated by the desire for robots to be able to handle situations where robots made of rigid components are not efficient, effective, or pose a threat to humans.^[3] Soft robots offer the promise of being able to interact more effectively with unknown objects and surroundings while operating with unlimited degrees of freedom.^[4] They may also be more mechanically robust and energy efficient than hard robots,^[5,6] and lightweight.^[7]

1. Introduction

Machines and robots provide value by performing tasks that humans are incapable of performing or by enhancing the ability of humans.^[1] Most robots are unable to adapt readily in new and


However, the inherent compliance of soft robots often makes it difficult for them to exert forces on surrounding surfaces or withstand mechanical loading. Controlled stiffness is an essential function in addressing this problem, enabling soft robots to apply large forces to their environments and to sustain external loads without significant deformations. Many technologies have been developed for stiffness tuning in soft devices,^[8] such as magnetorheological fluids,^[9] thermoplastics,^[10–12] shape-memory alloys and polymers,^[11,13–17] fluid polymer composites,^[18] or low melting point alloys (LMPAs).^[18–20] Among them, LMPAs are particularly attractive for soft robotic applications because their high electrical conductivity allows them to be used both as electrodes and circuits.^[21] LMPAs can be filled in microfluidic channels inside an elastomeric matrix,^[22–24] and thermal inputs can switch them between solid and liquid states, thereby changing the stiffness of the overall structure. This feature has enabled LMPAs to be combined with different types of soft actuators, such as dielectric elastomer actuators (DEAs),^[20,25] shape-memory alloy actuators,^[26] and pneumatic actuators.^[19] However, in these devices, the variable stiffness component and the actuation component of the robotic actuator are fabricated separately. This adds complexity to the device structure and the manufacturing process, thus limiting the range of possible designs.

In this article, we describe a new design solution and method to fabricate a soft, variable stiffness actuator with a shared electrode for both electrostatic actuation and variable stiffness, thus enabling a compact device structure that combines both functionalities. The device is actuated as a DEA, whereas the variable

E. Piskarev, V. Ramachandran, Prof. D. Floreano
Institute of Microengineering
School of Engineering
École Polytechnique Fédérale de Lausanne
1015 Lausanne, Switzerland
E-mail: dario.floreano@epfl.ch

Prof. J. Shintake
Department of Mechanical and Intelligent Systems Engineering
School of Informatics and Engineering
University of Electro-Communications
1-5-1 Chofugaoka, Chofu 182- 8585 Tokyo, Japan

N. Baugh, Prof. M. D. Dickey
Department of Chemical and Biomolecular Engineering
North Carolina State University
911 Partners Way, Raleigh, NC 27695, USA
E-mail: mddickey@ncsu.edu

 The ORCID identification number(s) for the author(s) of this article can be found under <https://doi.org/10.1002/aisy.202000069>.

© 2020 The Authors. Published by WILEY-VCH Verlag GmbH & Co. KGaA, Weinheim. This is an open access article under the terms of the Creative Commons Attribution License, which permits use, distribution and reproduction in any medium, provided the original work is properly cited.

DOI: 10.1002/aisy.202000069

stiffness functionality is provided by the shared electrode made of liquid metal (LM).

DEAs are a class of electroactive polymers that typically consist of an elastomeric dielectric layer and highly compliant electrodes, such as carbon conductive grease or a silicone mixture with carbon particles, which are applied to the polymer surface and do not constrain the motion of the polymer layer. Applying an electric potential across the electrodes generates an attractive electrostatic force that causes the elastomer to shrink in thickness and expand in the area. The elastic forces of the elastomer oppose this expansion. Thus, the final shape depends on the balance of these forces and ultimately provides a way to use the voltage applied to both compliant electrodes to change the shape of an elastomer. Due to the physical phenomena governing dielectric elastomers, they exhibit fast actuation rates with a bandwidth of 1 kHz and high efficiency up to 90% in energy harvesting.^[27,28] In addition, DEAs can be thin (up to 3 μm), lightweight (less than 1 g), and display actuation strains up to 1692% when voltage is applied.^[29,30] Moreover, they also provide the capabilities of electric switching and self-sensing.^[31,32] DEAs are now widely used for robotics and medical applications, including bioinspired robots,^[33–40] grippers, manipulators,^[4,41,42] and rehabilitation devices.^[43] In terms of fabrication approaches, DEAs are regularly manufactured by planar techniques: applicator coating,^[4] spin coating,^[44] and serial mechanical assembly.^[45]

LMPA is a phase-change material that has found application in wearables,^[46] medical applications,^[47] stretchable antennas,^[24] variable stiffness pneumatic actuators,^[19] and DEAs.^[20] LMPAs are attractive materials as they display stiffness change between rubbery and rigid states up to 9000 times,^[48] and fast (less than 1 s) phase change transition from a solid to a liquid state.^[22] Unfortunately, most of the manufacturing methods are laborious and time consuming, for example, support mold fabrication and metal injection^[20,22] or a multistep layered molding and casting process.^[19]

The variable stiffness dielectric elastomer actuators (VSDEAs) have been previously fabricated based on different variable stiffness technologies such as LMPAs^[20] shape-memory polymers (SMPs),^[16] and thermoplastics.^[12] Shintake et al.^[20] developed a VSDEA by merging together the DEA with the soft variable stiffness tissue. In this case, the variable stiffness change occurs due to the LMPA traces encapsulated into the silicone matrix.^[22] The use of LMPA allows achieving higher stiffness differences between soft and rigid states equal to 90 times. The fact that this actuator is composed of two separate devices leads to complexity in a structure. In addition, the fabrication process of each of the elements is long and complicated due to curing phases. McCoul et al.^[16] designed the VSDEA based on conductive SMP is composed of three variable stiffness segments that could independently be activated. In addition, the use of the conductive SMP layer at the same time as a ground electrode of DEA simplifies the structure. However, the reported stiffness change is low (the rigid state shows a 70% increase in force compared to the soft state) because of the thickness of the SMP layer equal to 300 nm. Furthermore, the fabrication process is long and complex because it requires preparation of SMP mixture and curing of electrodes and silicone layers. Yu et al.^[12] developed a VSDEA consisting of the thermoplastic as a dielectric layer and compliant electrodes made of carbon grease from both sides.

The thermoplastic layer can change a storage modulus under applied heat from 1.5 GPa at 30 °C to 0.42 MPa at 70 °C. However, the stiffness change coefficient and the bending stiffness of the actuator have not been presented by the authors. The actuation strain can be controlled by the applied electrical field with the maximum measured strain equal to 335% in the area expansion at 260 MV m⁻¹. As an application for the VSDEA, the Braille display has been developed. Actuators showed a fairly sharp transition between glassy and rubbery states equal to 40 s. The potential use of the actuator as a gripper and its performance in terms of bending angle has not been discussed.

The actuator is composed of a variable stiffness layer made of a LM (gallium), which also serves as an electrode layer for the DEA. The cofabricated electrode results in a comparatively lighter structure and a higher stiffness change ratio per device mass. The VSDEA described in this article is fabricated using off-the-shelf materials and a layer-by-layer process without curing. Together with the simplicity of the architecture of the device, the fabrication process is simpler, easier, and faster than those of previous studies.^[16,20]

2. VSDEA Structure and Working Mechanism

The structure and working principle of the VSDEA are shown in **Figure 1**. It consists of four layers. The first layer is a serpentine channel filled with gallium that serves as the upper electrode for the electrostatic actuation and, at the same time, as a variable stiffness component. The channel is encapsulated in an elastomer film. The second layer is a prestretched elastomer film that serves as a dielectric for the electrostatic actuation. The third layer is made of carbon grease that acts as the positive electrode for the electrostatic actuation. The fourth layer is an inextensible polypropylene material that prevents elongation of the structure. When the four layers are joined, the dielectric layer bends to adopt the curvature with the lowest potential energy.

When there is no input (the power supply is off, and the serpentine shape with LM is not Joule heated), gallium in the channel is solid, and the device is rigid (**Figure 1b-i**). By applying direct Joule heating, the gallium electrode changes its state from solid (rigid) to liquid (soft) (**Figure 1b-ii**). In the soft state, the VSDEA can actuate from a curled shape to a flat shape by applying a high voltage across the device (**Figure 1b-iii**). In the absence of Joule heating, the electrode freezes and keeps the VSDEA in a flat state without the need for voltage input (**Figure 1b-iv**).

3. Fabrication Process

The fabrication process of the VSDEA is shown in **Figure 2**. A double-sided tape (VHB 4905, 500 μm thick) is used as an elastomeric matrix to encapsulate the LM electrode.

A layer of the VHB is attached temporarily to a polymethyl methacrylate (PMMA) plate to facilitate handling and processing. Then, another VHB layer is attached to the first layer so that the red liner of the second VHB is stuck to the first one (**Figure 2a**). After that, an air gun is used as a noncontact method to force the VHB layer against the liner. The entire surface of the second VHB layer is ablated to a depth of 220 μm by a CO₂ laser (**Figure 2b**). This step helps to improve interfacial adhesion

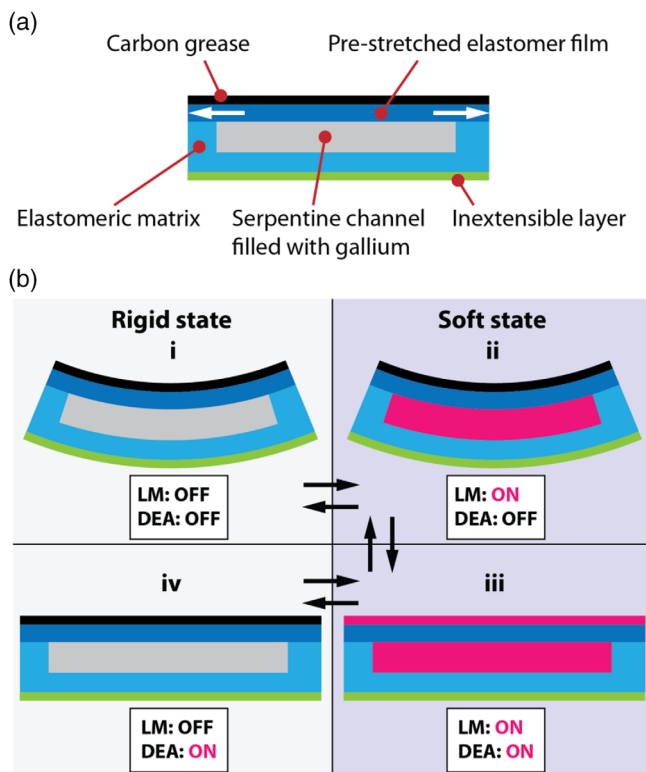


Figure 1. Working principle of VSDEA. a) The actuator design: pre-stretched VHB layer is attached to the matrix with serpentine shape made of VHB. The LM inside the serpentine shape and the carbon grease on the prestretched VHB work as electrodes of DEA. The bottom inextensible layer is connected to VHB matrix. b) i) The VS part of VSDEA is rigid, and DEA is deactivated. ii) The activation of LM changes the stiffness of VSDEA, therefore, the device becomes soft. iii) The activation of DEA leads to compression of the elastomer layer made of VHB (brown). The squeezing in one direction leads to expansion of the surface of elastomer layer which allows the DEA to change the shape from the bent to flat shape. iv) The following shutdown of LM layers makes the VSDEA completely rigid.

for reasons we are still trying to elucidate but may have to do with the enhanced surface area. Subsequent to the ablation, a serpentine shape is engraved into the surface of VHB.

Then, a dielectric layer (VHB F9473PC, 250 μm thick) is laminated onto another film stack (Figure 2c). Afterward, this layer is engraved via CO_2 laser ablation with a depth of 70 μm (Figure 2d). The dielectric layer is prestretched to 125% strain and adhered to the film stack (Figure 2e). The matrix of VHB made in the previous steps (Figure 2a,b) is inverted and put on the prestretched dielectric layer (Figure 2f). An inextensible layer (Scotch tape, 50 μm thick) is attached to the VHB to prevent elongation. At this point, the dielectric curls until it reaches its minimum potential energy configuration. The bonding between VHB and the inextensible layer is sufficiently robust, and we never observed delamination in any of the experiments. The microchannels inside the VHB matrix are injected with liquid gallium using a syringe. The actuator is then cut to remove excess elastomer (Figure 2g). After that, the sample is flipped, and carbon grease is cast on the dielectric layer. The thickness of this

carbon grease layer is around 130 μm and serves the DEA electrode, where a positive high voltage is applied. To establish electrical connections, a conductive tape is attached to the carbon grease, and copper wires are inserted into the gallium (Figure 2h). The copper wires serve two purposes: 1) they connect the serpentine gallium electrode with an external power supply and, at the same time 2) they provide a nucleation site for gallium crystals to form at room temperature. Without a nucleation site, the gallium remains liquid at room temperature due to its supercooling characteristics.^[49] The fabrication process described here is suitable for batch manufacturing. In this study, all the VSDEAs are manufactured in groups of four. In the device, all the layers stick to each other due to the high bonding strength between acrylic adhesives. Moreover, this adhesion does not require any additional glue, thus further simplifying the layer-by-layer manufacturing process.

The fabricated VSDEA (Figure 3a) has dimensions of 57 mm \times 12.2 mm \times 0.9 mm and weighs 0.7 g. The active area of the electrodes is 30 mm \times 8 mm, and the line width of channel is 0.96 mm. The distance between the channels equals to 0.45 mm. The thickness of the LM channel is 0.28 mm. The serpentine shape is etched on the VHB layer with a size of 57 mm length \times 12.2 mm width. The VHB has 2.1 mm of width on each side of the channels to encapsulate the serpentine shape faultlessly. This additional width also prevents possible delamination between two VHB layers. The serpentine shape has two openings, one at the start and one at the end of the channel, which are made by laser engraving with a 1.5 mm diameter. Figure 3b left shows the actuator in its initial state where both the DEA and the LM are off. In this rigid state, the device can withstand external loading (a nut). Figure 3b right shows the actuator in the active state where the DEA is off and LM is on. The uniformity of the stiffness over the device area depends on the homogeneity of the cross-sectional area along the length of the device, which is achieved by the use of off the shelf materials, layer-by-layer fabrication process, and precise laser engraving.

A cross-section of the VSDEA is shown in Figure 3c where one can see the inextensible layer (50 μm thick), the VHB layer containing the microchannel (500 μm thick), dielectric layer (250 μm thick), and the carbon grease layer (130 μm thick). The total thickness of the VSDEA is 930 μm .

4. Results and Discussion

We characterized the device in terms of transition time between the two states (i.e., response time), stiffness change between rigid and soft states, and performance as maximum bending angle and output force.

We first characterized the response time between the rigid and soft states. From the rigid state, it took 8.5 s to reach the soft state with an applied power of 3.96 W. In the soft state, the VSDEA had an elastic modulus of 0.11 MPa. After removing input power, it took 663 s to return to the rigid state. The result shows that there is a tradeoff in the transition time of the two states. As the melting point of gallium is around 29 $^\circ\text{C}$, the thermal driving force required for achieving the soft state is small at ambient temperature, and therefore the transition time is short. In contrast, for the same reason, the transition time from the soft to rigid state

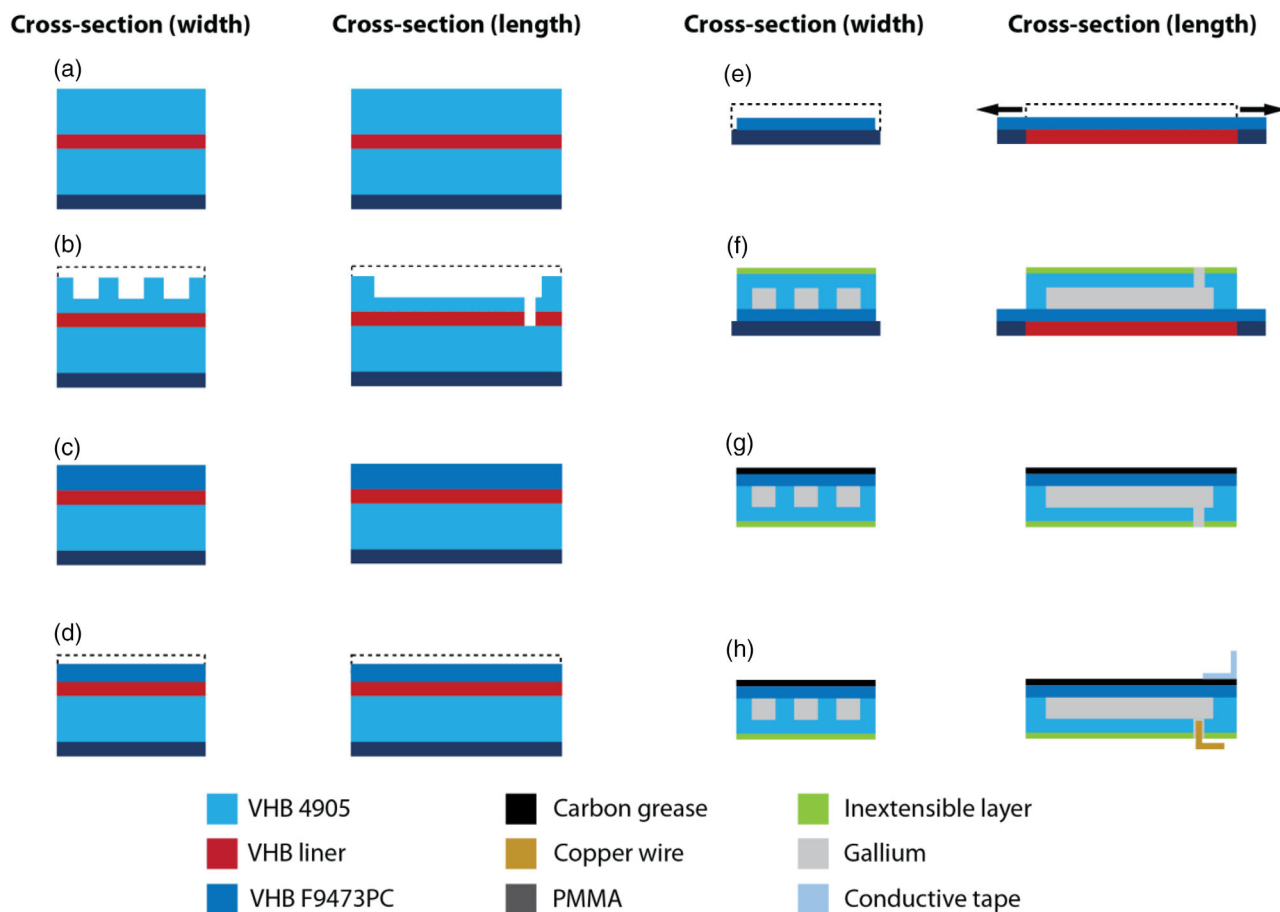


Figure 2. Fabrication process of VSDEA. a) VHB 4905 is attached to the support VHB layer and PMMA plate. b) Microchannels are engraved on the surface of VHB 4905. c) VHB F9473PC is stuck to the support VHB and PMMA plate to be etched in the step d). e) The elastomer layer is prestretched. f) The VHB 4905 is stuck onto VHB F9473PC dielectric elastomer layer. Then the inextensible layer is attached onto VHB 4905 and LM is injected via syringe. g) The actuator is flipped and the carbon grease is attached to the surface. h) Electrical connections are applied to both electrodes.

tends to belong. This behavior could be adjusted, in principle, using melting point alloys with a higher melting point such as Cerrolow 117.^[20,22,47]

We then investigated the stiffness change of the VSDEA by collecting and comparing the measured reaction force of rigid and soft states as a function of the forced displacement. In this test, the actuator was held in a universal testing machine (Instron, 3340). The machine pulled the vertically oriented VSDEA to change the bending angle of the device while measuring the reaction force as a function of the displacement. The result is shown in **Figure 4a**. The reaction force is larger in the rigid state than in the soft state. To quantify the rigidity of the device, spring constant was calculated as a ratio of the reaction force and the forced displacement by linear fitting of the data. For the rigid and soft states, the spring constants were 34.7 and 0.2 N mm⁻¹, respectively. These values correspond to a stiffness change factor (SCF) of 183, which is significantly larger than that of other types of VSDEA, which exhibit at best 90-time stiffness change.^[16,20] Moreover, when the stiffness change per mass of this VSDEA is 261 times g⁻¹ (device mass 0.7 g), which is even higher than that of previous work (90 times g⁻¹).^[16,20] To explain why the new design has higher

stiffness change compared with the previous, we compare the theoretical calculations of SCF for the current device and the reference one.^[20] The structures of the VSDEAs are considered as a composite with a layer-by-layer structure. Each layer represents the electrode made of LM, the dielectric layer, encapsulation layer, etc. The approach to calculate the effective Young's modulus and the total second moment of the area for each of the cross-sections is based on the studies reported in the literature.^[22,50]

The SCF is defined as the ratio between the bending stiffness of the VSDEA in the rigid state and the soft state. The SCF is higher for the VSDEA in the work presented here compared with the previous work due to the stiffness change in the LM DEA electrode.^[20] The VSDEA is a composite structure composed of multiple layers, including the LM electrode, the dielectric, and the encapsulation. The effective bending stiffness of the structure, k is computed using the relation, $k = \sum 3E_i I_i / L_i^3$ where E_i is the Young's modulus, I_i is the second moment of area ($I = wh^3/12$, where w is width and h is thickness), and L_i is the length of the i th layer. As defined earlier, the SCF is given by the relation, $SCF = k_r / k_s$ where k_r and k_s are the bending stiffnesses of the VSDEA in the rigid and soft states.

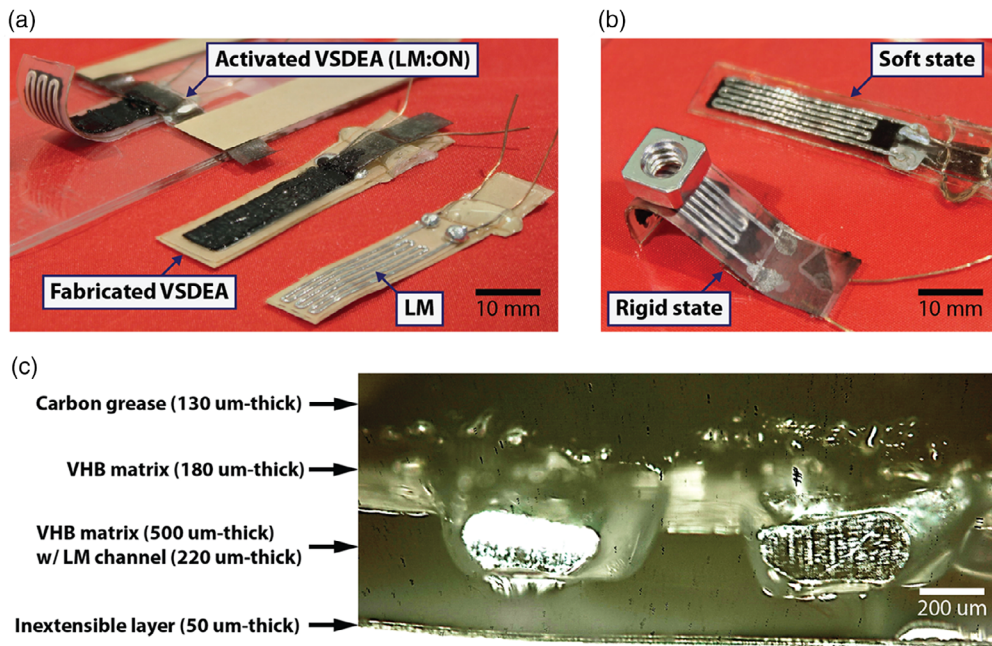


Figure 3. a) Fabricated VSDEA with an activated variable stiffness layer (left), VHB membrane with injected gallium (right), b) VSDEA with activated DEA and gallium layer (on the top), VSDEA in the initial state with nonactive LM layer (on the bottom), c) VSDEA cross-sectional annotation (top to bottom): carbon grease layer, dielectric, VHB matrix, inextensible layer. The active area of the electrodes is $30 \text{ mm} \times 8 \text{ mm}$ and the line width of channel is 0.96 mm . The distance between the channels equals to 0.45 mm .

For the current VSDEA, $E_{LM} = 9.8 \text{ GPa}$ (rigid) $I_{LM} = 0.005 \times 10^{-12} \text{ m}^4$, $E_{VHB} = 5 \times 10^5 \text{ Pa}$, $I_{VHB} = 0.48 \times 10^{-12} \text{ m}^4$, $L_{LM} = L_{VHB} = 30 \text{ mm}$ gives us a $k_r = 5.44 \text{ N m}^{-1}$, $k_s = 0.027 \text{ N m}^{-1}$, and $\text{SCF} = 201$. In the previous study,^[20] the VSDEA had $E_{LM} = 3.0 \text{ GPa}$ ^[22] (rigid) $I_{LM} = 0.0081 \times 10^{-12} \text{ m}^4$, $E_{sil} = 330 \times 10^3 \text{ Pa}$, $I_{sil} = 0.83 \times 10^{-12} \text{ m}^4$, $L_{LM} = L_{VHB} = 29 \text{ mm}$ that gave us a $k_r = 2.6 \text{ N m}^{-1}$, $k_s = 0.03 \text{ N m}^{-1}$, and $\text{SCF} = 86.6$. The E_{LM} in the soft state is negligible. As shown earlier, the bending stiffness of the VSDEA in the rigid state for the device presented in this work is greater than twice the same in the earlier work.^[20] The difference between the empirical SCF and the theoretical values could be caused by the fabrication process, e.g., the shrinking forces of the VHB substrate are squeezing the LM channels, thus, decreasing the width of the LM channels. It is worth noting that the amount of LM is $\approx 2 \times$ higher in this work. However, the density of gallium (5813 kg m^{-3}) used in this study is lower than the density of Cerrolow 117 (8858 kg m^{-3}) used in the previous work. This leads to the SCF per mass of the device as $261 \times \text{g}^{-1}$, which is 2.6 times higher than the previous work without the shared electrode.

We next assessed the actuation performance of the VSDEA. For this purpose, a high voltage power supply has been used in addition to the low voltage one, which is used to control the stiffness change. The integration penalty of working with two independent power sources could be further solved by reduction of the voltage of DEA and, at the same time, increase in the voltage for the stiffness change. The former challenge could be overcome by reducing the thickness of the dielectric layer and the latter could be achieved by increasing of the electrical resistance of the LM electrode layer. Finally, the new

configuration allows driving both functionalities at the order of 100 V .^[51]

Figure 4b shows the actuator's bending angle as a function of the applied voltage. In the soft state, the actuator displays a deflection of 31° at 3 kV compared with 23° at the same voltage observed in the other type of VSDEA with LMPA.^[20] This enhanced actuation performance with respect to previous work, can be explained by the smaller thickness of the cofabricated electrode, which has comparatively wider microchannels (Figure 3c), thus resulting in smaller momentum of inertia. In our study, the width of the serpentine shape is maximized to increase the active area where two electrodes (carbon grease and serpentine shape) overlap to enhance the performance of the electrostatic actuation. In addition, there is a tradeoff between the thickness of the electrodes. Lower thickness of the electrodes leads to the reduction of encapsulation layers, and thus, a maximization of energy density. In contrast, the incidental outcome is the decrease in the cross-sectional segments with metal, resulting in a drop in the SCF. In the rigid state, the actuation angle is only 1.3° at 3 kV . The actuation angle of the VSDEA also shows high repeatability with a low hysteresis in a five-cycle test where three different actuators were tested (Figure 4c) from 0 V to 3 kV with the step of 500 V . The value in blue or pink triangles represents the average value of actuation stroke angle during five-cycle test for one-half of the cycle: increasing or decreasing the voltage. Values consider three tested actuators and five cycles per each actuator. The same approach has been further used to evaluate the repeatability of the blocked force during a five-cycle test (Figure 4e).

Further, we investigated the output force generated by the VSDEA as a function of applied voltage (Figure 4d). The rigidity

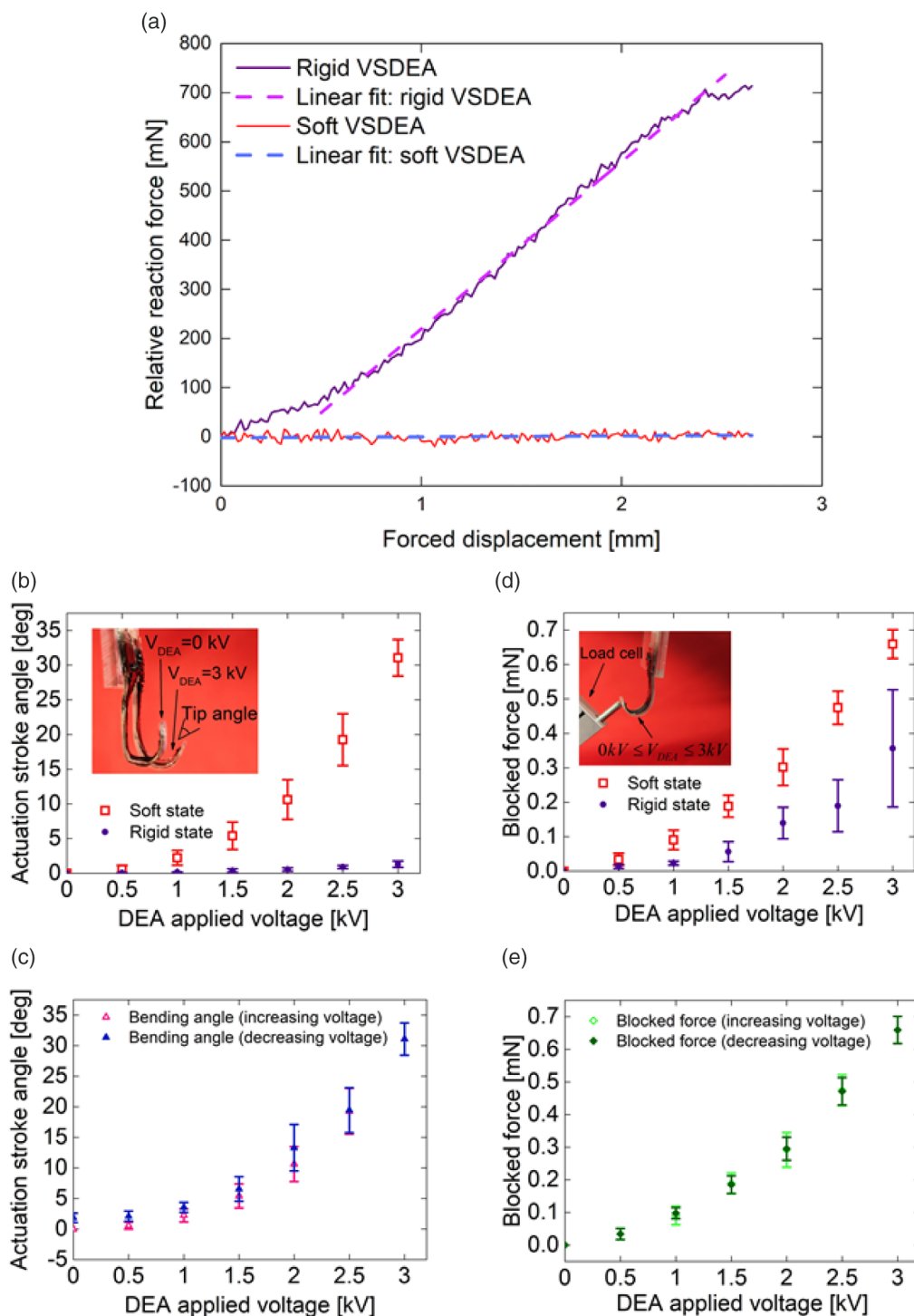


Figure 4. The measured response of the fabricated VSDEA actuator under an applied voltage. a) Reaction force versus forced displacement. For the rigid and soft states, the spring constants were 34.7 and 0.2 N mm^{-1} , respectively. These values correspond to a SCF of 183. b) Actuation stroke angle versus applied voltage in the rigid and soft states. The actuator displays a deflection of 31° and 1.3° at 3 kV in the soft and rigid states, respectively. c) Five-cycle test: actuation stroke angle versus applied voltage in the soft state. d) Blocked force versus applied voltage in the soft and rigid states. e) Five-cycle test: blocked force versus applied voltage in the soft state. The values in (c,e) represent the average value of actuation stroke angle and blocked force after five-cycle test for one-half of the cycle: increasing or decreasing the voltage. Values consider three tested actuators and five cycles per each actuator.

of LM does not affect the blocked force values because it only depends on the design of the actuator and applied voltage. Hence, the collected data of blocked force in the rigid state show nearly the same values as in the soft state. The blocked force displays a maximum value of 0.65 mN in the soft state (Figure 4d). The force in the rigid state displays a lower value (0.36 mN). This is because the actuated angle of the device is tiny in the rigid state (1.3°), which limits the stroke necessary to push the load cell. For the same reason, the deviation of the data in this state is more significant. Similar to the case of the actuation angle, the VSDEA shows excellent repeatability of the force during a five-cycle test (Figure 4e, an average of three samples).

The blocked force can be improved by increasing the electrostatic force (i.e., Maxwell stress) generated from the actuator. For this purpose, the thickness of the dielectric layer can be decreased, or the applied voltage can be increased. In this work, the thickness of the dielectric layer is 0.18 mm which is engraved from the initial thickness of 0.25 mm. We have tried to further decrease the thickness of dielectric layer; however, we have found that it is limited as the material burst under the heat of a laser. One of the possible solutions is to find a commercially available acrylic sticky tape with a thickness lower than 0.18 mm and use it directly in the next version of the design.

5. Conclusions

The novelty of the VSDEA described in this article consists of using a shared electrode for both electrostatic actuation and variable stiffness in a single device structure. This approach simplifies the architecture of variable stiffness actuators, where the stiffness control component and the actuation components are two different structures. The fabrication process of the presented VSDEA is simpler. It can be made by a rapid layer-by-layer process without the use of any glue thanks to the enhanced bonding strength between two substrate layers of acrylic double-sided sticky tape. The proposed VSDEA displays significantly higher stiffness change and actuation performance compared with a VSDEA with different stiffness and actuation structures, resulting in a stiffness change per mass that is almost three times higher.

The implementation of high variable SCF leads to the comparatively long transition time from soft to rigid state. While this may not be a problem in some applications, it would be effective to modify the geometries of the device to shorten the transition. For example, the serpentine shape of the VSDEA could be redesigned to maximize the surface area by decreasing the cross-sectional area and lengthening of the overall microchannel, which is expected to speed up the rigidifying process. The presented strategy using cofabricated electrode could be applied to other variable stiffness devices that are composed of cured encapsulation structures with polymer membranes, such as, those based on shape-memory polymers and layer-jamming devices.^[16,52] The structure of these devices will be simplified, thus making their fabrication faster and easier. The same benefits can be exploited in the development of other robotic applications where variable stiffness functionality, such as, grippers and haptic devices are becoming increasingly essential.^[4,53] Along with the optimization, the variable stiffness actuators with

cofabricated electrodes will be applied to various devices to investigate its versatility, which is expected to bring highly functional soft robotic applications.

6. Experimental Section

The electrical input and output of the serpentine electrode made of gallium were connected to a power supply (Extech, 382213). In addition, the same electrode was connected to the ground of a high voltage power supply that consisted of a waveform generator, 20 MHz (Keysight Technologies, 33220 A), digital multimeter (Keithley Instruments, 2400), and a high-voltage power amplifier (Trek, 609E-6). Another electrode made of carbon grease was connected only to the positive terminal of the high-voltage power supply. The mechanical characterization of VSDEA in terms of bending angle and blocked force was carried out with a camera (Canon, EOS Rebel T1i) and a precision gram load cell (Transducer Techniques, GSO series) connected to a smart digital panel (Transducer Techniques, DPM-3). The blocked force and bending angle characterization were done separately with the voltage step of 500 V. For the bending angle measurements, pictures were taken and processed by a script in MATLAB. For the measurement of the reaction force of the rigid and soft VSDEA as functions of the forced displacement, the actuator was held in a universal testing machine (Instron, 3340). The testing machine pulled the VSDEA, resulting in a change of the device's bending angle. A camcorder recorded all tests to define an interval of 3–5 mm where the angle change was seen. Later, the acquired data was processed by MATLAB.

Acknowledgements

This work was supported by the SNSF Bridge project 20B2-1 180861. This work was partially supported by the Japanese Ministry of Education, Culture, Sports, Science, and Technology through the Leading Initiative for Excellent Young Researchers (LEADER). The authors thank Jiayi Yang and Amber Hubbard for their help with the manuscript and pictures.

Conflict of Interest

The authors declare no conflict of interest.

Keywords

dielectric elastomer actuators, gallium, liquid metals, soft robotics, variable stiffnesses

Received: April 7, 2020

Revised: June 19, 2020

Published online:

- [1] M. Decker, M. Fischer, I. Ott, *Rob. Auton. Syst.* **2017**, *87*, 348.
- [2] D. Rus, M. T. Tolley, *Nature* **2015**, *521*, 467.
- [3] G. M. Whitesides, *Angew. Chem. Int. Ed.* **2018**, *57*, 4258.
- [4] J. Shintake, S. Rosset, B. Schubert, D. Floreano, H. Shea, *Adv. Mater.* **2016**, *28*, 231.
- [5] B. S. Homborg, R. K. Katzschmann, M. R. Dogar, D. Rus, *Auton. Robots* **2019**, *43*, 681.
- [6] L. Shui, L. Zhu, Z. Yang, Y. Liu, X. Chen, *Soft Matter* **2017**, *13*, 8223.
- [7] M. Zhang, G. Li, X. Yang, Y. Xiao, T. Yang, T.-W. Wong, T. Li, *Smart Mater. Struct.* **2018**, *27*, 095016.
- [8] L. Wang, Y. Yang, Y. Chen, C. Majidi, F. Iida, E. Askounis, Q. Pei, *Mater. Today* **2018**, *21*, 563.

- [9] J. A. Jackson, M. C. Messner, N. A. Dudukovic, W. L. Smith, L. Bekker, B. Moran, A. M. Golobic, A. J. Pascall, E. B. Duoss, K. J. Loh, C. M. Spadaccini, *Sci. Adv.* **2018**, *4*, eaau6419.
- [10] L. Wang, U. Culha, F. Iida, *Bioinspir. Biomim.* **2014**, *9*, 016006.
- [11] S. I. Rich, V. Nambesan, R. Khan, C. Majidi, *J. Intell. Mater. Syst. Struct.* **2019**, *30*, 2908.
- [12] Z. Yu, W. Yuan, P. Brochu, B. Chen, Z. Liu, Q. Pei, *Appl. Phys. Lett.* **2009**, *95*, 192904.
- [13] Y. Yang, Y. Chen, Y. Li, M. Z. Q. Chen, Y. Wei, *Soft Robot.* **2017**, *4*, 147.
- [14] A. Firouzeh, M. Salerno, J. Paik, *IEEE Trans. Robot.* **2017**, *33*, 765.
- [15] Y.-F. Zhang, N. Zhang, H. Hingorani, N. Ding, D. Wang, C. Yuan, B. Zhang, G. Gu, Q. Ge, *Adv. Funct. Mater.* **2019**, *29*, 1806698.
- [16] D. McCoul, S. Rosset, N. Besse, H. R. Shea, *Smart Mater. Struct.* **2017**, *26*, 025015.
- [17] Y. Qiu, Z. Lu, Q. Pei, *ACS Appl. Mater. Interfaces* **2018**, *10*, 24807–24815.
- [18] Y. Shan, M. Philen, A. Lotfi, S. Li, C. E. Bakis, C. D. Rahn, K. W. Wang, *J. Intell. Mater. Syst. Struct.* **2009**, *20*, 443.
- [19] Y. Hao, T. Wang, L. Wen, in *Lecture Notes Computer Science (Including Subseries Lecture Notes Artificial Intelligence and Lecture Notes in Bioinformatics)*, Springer Verlag, Berlin, **2017**, pp. 151–161.
- [20] J. Shintake, B. Schubert, S. Rosset, H. Shea, D. Floreano, *IEEE Int. Conf. Intell. Robot. Syst.* **2015**, *2015*, 1097.
- [21] M. D. Dickey, *Adv. Mater.* **2017**, *29*, 1.
- [22] B. E. Schubert, D. Floreano, *RSC Adv.* **2013**, *3*, 24671.
- [23] A. C. Siegel, D. A. Bruzewicz, D. B. Weibel, G. M. Whitesides, *Adv. Mater.* **2007**, *19*, 727.
- [24] J.-H. So, J. Thelen, A. Qusba, G. J. Hayes, G. Lazzi, M. D. Dickey, *Adv. Funct. Mater.* **2009**, *19*, 3632.
- [25] J. Wissman, L. Finkenauer, L. Deseri, C. Majidi, *J. Appl. Phys.* **2014**, *116*, 144905.
- [26] W. Wang, S.-H. Ahn, *Soft Robot.* **2017**, *4*, 379.
- [27] R. D. Kornbluh, R. Pelrine, Q. Pei, S. Oh, J. Joseph, in *Smart Struct. Mater. 2000 Electroact. Polym. Actuators and Devices (EAPAD)* (Ed.: Y. Bar-Cohen), SPIE, San Diego, CA **2000**, pp. 51–64.
- [28] J.-P. L. Bigue, J.-S. Plante, *IEEE/ASME Trans. Mechatronics* **2013**, *18*, 169.
- [29] A. Poulin, S. Rosset, H. Shea, in *Proc. of Electroactive Polymer Actuators and Devices (EAPAD)* (Eds.: Y. Bar-Cohen, F. Vidal), SPIE, Las Vegas, NV **2016**, p. 97980L.
- [30] T. Li, C. Keplinger, R. Baumgartner, S. Bauer, W. Yang, Z. Suo, *J. Mech. Phys. Solids* **2013**, *61*, 611.
- [31] I. A. Anderson, T. A. Gisby, T. G. McKay, B. M. O'Brien, E. P. Calius, *J. Appl. Phys.* **2012**, *112*, 041101.
- [32] T. A. Gisby, E. P. Calius, S. Xie, I. A. Anderson, in *Proc. of Electroactive Polymer Actuators and Devices (EAPAD)* (Ed.: Y. Bar-Cohen), SPIE, San Diego, CA **2008**, p. 69271C.
- [33] R. Pelrine, R. D. Kornbluh, P. Qibing, S. Stanford, O. Seajin, J. J. Eckerle, R. J. Full, M. A. Rosenthal, K. Meijer, Q. Pei, S. Stanford, S. Oh, J. J. Eckerle, R. J. Full, M. A. Rosenthal, K. Meijer, in *Procwe* (Ed.: Y. Bar-Cohen), **2002**, pp. 126–137.
- [34] C. T. Nguyen, H. Phung, T. D. Nguyen, C. Lee, U. Kim, D. Lee, H. Moon, J. Koo, J. Nam, H. R. Choi, *Smart Mater. Struct.* **2014**, *23*, 065005.
- [35] M. T. Petralia, R. J. Wood, in *2010 IEEE/RSJ Int. Conf. Intell. Robot. Syst.* IEEE, Piscataway, NJ **2010**, pp. 2357–2363.
- [36] G. Gu, J. Zou, R. Zhao, X. Zhao, X. Zhu, *Sci. Robot.* **2018**, *3*, eaat2874.
- [37] T. Li, G. Li, Y. Liang, T. Cheng, J. Dai, X. Yang, B. Liu, Z. Zeng, Z. Huang, Y. Luo, T. Xie, W. Yang, *Sci. Adv.* **2017**, *3*, e1602045.
- [38] C. T. Nguyen, H. Phung, P. T. Hoang, T. Dat Nguyen, H. Jung, H. Moon, J. C. Koo, H. R. Choi, in *2017 IEEE/RSJ Int. Conf. Intell. Robot. Syst.*, IEEE, Piscataway, NJ **2017**, pp. 6233–6238.
- [39] Y. Tang, L. Qin, X. Li, C.-M. Chew, J. Zhu, in *2017 IEEE/RSJ Int. Conf. Intell. Robot. Syst.*, IEEE, Piscataway, NJ **2017**, pp. 2403–2408.
- [40] L. Xu, G. Gu, in *2017 24th Int. Conf. Mechatronics Mach. Vis. Pract.* IEEE, Piscataway, NJ **2017**, pp. 1–3.
- [41] O. A. Araromi, I. Gavrilovich, J. Shintake, S. Rosset, M. Richard, V. Gass, H. R. Shea, *IEEE/ASME Trans. Mechatronics* **2015**, *20*, 438.
- [42] S. Shian, K. Bertoldi, D. R. Clarke, *Adv. Mater.* **2015**, *27*, 6814.
- [43] T. Dong, X. Zhang, T. Liu, *Front. Inf. Technol. Electron. Eng.* **2018**, *19*, 1303.
- [44] M. Duduta, R. J. Wood, D. R. Clarke, *Adv. Mater.* **2016**, *28*, 8058.
- [45] H. Zhao, A. M. Hussain, M. Duduta, D. M. Vogt, R. J. Wood, D. R. Clarke, *Adv. Funct. Mater.* **2018**, *28*, 1804328.
- [46] A. Tonazzini, S. Mintchev, B. Schubert, B. Mazzolai, J. Shintake, D. Floreano, *Adv. Mater.* **2016**, *28*, 10142.
- [47] C. Chautems, A. Tonazzini, Q. Boehler, S. H. Jeong, D. Floreano, B. J. Nelson, *Adv. Intell. Syst.* **2019**, *1900086*, 1900086.
- [48] W. Shan, T. Lu, C. Majidi, *Smart Mater. Struct.* **2013**, *22*, 085005.
- [49] D. Campanini, Z. Diao, A. Rydh, *Phys. Rev. B* **2018**, *97*, 184517.
- [50] J. Shintake, *Ph.D. Thesis*, École polytechnique fédérale de Lausanne, **2016**.
- [51] A. Poulin, S. Rosset, H. R. Shea, *Appl. Phys. Lett.* **2015**, *107*, 244104.
- [52] A. Tonazzini, J. Shintake, C. Rognon, V. Ramachandran, S. Mintchev, D. Floreano, *RoboSoft*, **2018**, pp. 485–490.
- [53] J. Shintake, E. Piskarev, S. H. Jeong, D. Floreano, *Adv. Mat. Tech.* **2017**, *3*, 1700284.